71st Conference of the Italian Thermal Machines Engineering Association, ATI2016, 14-16 September 2016, Turin, Italy

PM$_{10}$ Dispersion Modeling by means of CFD 3D and Eulerian– Lagrangian models: Analysis and comparison with experiments

S. Brusca[a], F. Famoso[b], R. Lanzafame[b], S. Mauro[b], M. Messina[b], S. Strano[b]*

[a]University of Messina, C.da Di Dio, Messina, 98166, Italy
[b]University of Cataia, V.le A. Doria 6, Catania 95125, Italy

Abstract

This research deals with the analysis of the dispersion of PM$_{10}$ by using fluid-dynamic simulation framework. Firstly, an experimental campaign was made in a wind tunnel. A cylindrical emitter of PM$_{10}$ was characterized in terms of PM$_{10}$ mass flow rate and outlet velocity. It was positioned in the wind tunnel chamber where several sensors were also placed downwind. The use of different sensor configurations allowed the evaluation of the PM$_{10}$ concentrations in several locations. The experimental campaign was reproduced in ANSYS-Fluent, by recreating in Design-Model, a 3D geometries of the test case. Different calculation grids were tested in order to find the proper balance between computing time and accuracy. The CFD 3D model was based on the Eulerian approach for the continuous phase and Lagrangian approach for the dispersion phase setting the DPM for the evaluation and dispersion of particulate matters. The turbulence was solved by using a k-ε RANS approach and a quite advanced unsteady DES model. Several simulations were carried out by varying the flow inlet velocities in configurations with and without obstacles. The results obtained from the post-processing phase were then compared with the experimental campaign. With obstacles a PM concentration increment is observed at all imposed air velocity because of recirculation phenomena generated around the obstacles.

Keywords: 3D CFD model; Eulerian/Lagrangian particle dispersion model; air pollution; aerosol particles.

---

* Corresponding author. Tel.: +39 095 7382455; Fax: +39 095 738464.
  E-mail address: sstrano@dii.unict.it

1. Introduction

The rapid economic and industrial growth of many countries in the last decade has led to an expansion of urban areas, and above all, a tremendous increase of energy consumption and emissions of air pollutants. Air pollution has become one of the world's worst problems of toxic pollution particularly for the consequences it has on the socio-medical systems [1]. Many countries have developed some short-term and long-term strategies in order to reduce and control pollutant emissions in urban areas. Perhaps, one of the most important is the European Directive 2008/50/CE whose aim is to adopt a standardized method to control, monitor and study air pollutants in urban areas.

Among all possible air pollutants, the attention has recently shifted to Ozone (O_3), nitrogen dioxide (NO_2) and above all, the particulates (PM_{10}, $PM_{2.5}$). In general, particulate air pollution is a mixture of solid, liquid or solid and liquid particles suspended in the air. They are strictly correlated to anthropogenic activities, such as combustion of fossil fuels from stationary sources [2] and gas emissions from motor vehicles [3, 4]. It has been seen how they are also correlated with some climate conditions [5, 6]. These health consequences of aerosol and gas emissions in urban areas [7] has induced the scientific community to study air pollution dispersion and develop models to foresee trajectories of pollutants. Dispersion models use mathematical equations, describing atmosphere, chemical and physical processes to calculate concentrations, usually caused by some plume emission such as industrial chemistries, at various locations. There are many types of models, most of them are useful for some applications and less precise for others. For short-range local problems simple Gaussian type models have generally been used. These models are applicable for pollutant emissions into uniform atmospheric floors. They are based on Gaussian distribution of the plume and work in steady state conditions. Moreover, they are widely used in regulatory purposes because of their near real time solutions [8]. Unfortunately, these models are not suitable for predicting flow and concentration in complex urban or industrial areas, which are the places where aerosol particles are of major concern at present.

Today, thanks to the increasing CPU power, the use of Computational Fluid Dynamics (CFD) is rapidly imposing in the industrial risk assessment area as well. It is replacing integral models when particular situations, such as those involving complex terrains or large obstacles, are involved. This new approach in general will consider turbulent conditions caused by obstacles, barriers or buildings and work in non-steady states. There are usually two possible approaches in CFD to predict pollutants flows: Lagrangian and Eulerian methods. Lagrangian approach treats the fluid phase as continuum and the particulate second phase as single particles. In the Eulerian approach, the two phases, gas and particles are considered as interpenetrating continua coupled together by exchanging coefficients. Both of them have been used recently in many numerical and experimental studies involving complex terrain models [9, 10].

This paper deals with the implementation of a 3D CFD Eulerian/Lagrangian model to predict PM_{10} dispersion in a controlled system. The Eulerian approach was used for the continuous phase and Lagrangian approach, setting the Discrete Phase Model (DPM) to simulate particles trajectories. The turbulence was solved with a steady k-ε RANS approach for the case without obstacle and with an accurate unsteady DES model for the case with obstacles, in order to capture the large scale wake eddies which greatly influenced the particulate dispersion. The numerical results were treated and compared with experimental results from tests conducted in a wind tunnel.

Nomenclature

CFD   Computational Fluid Dynamics
PM   Particulate Matter
DPM   Discrete Phase Model
RANS   Reynolds-Averaged Navier Stokes
DES   Detached Eddie Simulation
L   Emitter Height

2. Experimental set-up

In order to calibrate 3D CFD models and verify their accuracy, a specific experimental set-up was implemented in the test chamber of a wind tunnel. In more detail, the experimental set-up consists of the following parts:

- A wind tunnel [11];
- A wood case [12];
- A PM_{10} emitter [12];
- A PM_{10} measurement and registration system [12].

The wind tunnel used has a test chamber 500 mm high, 500 mm wide and 1130 mm long and a variable air velocity between 0 and 30 m/s. More details about the wind tunnel used are provided in [11].

The wood case is essentially a plane that fits exactly on the bottom of the wind tunnel test chamber and acts as ground.

The PM_{10} emitter consists of a cylindrical chimney with controlled mass flow rate and velocity. The emitter of PM_{10} was characterized in terms of PM_{10} mass flow rate and plume initial velocity. PM emission system characterization and validation procedures are reported in [12]. The main characteristics of PM_{10} emitter are reported in Table 1.

Table 1. PM10 emitter main characteristics.

Description	Value
Height	90 mm
Diameter	20 mm
Outlet velocity	0.6 m/s
PM_{10} mass flow rate	10 – 30 μg/s

The PM_{10} measurement and registration system consists of a grid of three PM_{10} sensors on the ground plane. Aerocet-531S Mass Particle Counters were used as sensors [13]. The main characteristics of Aerocet-531S Mass Particle Counters are reported in Table 2. As it is possible to observe in Fig. 1, a schematic sketch of the implemented experimental set-up is shown, where all the elements of the case were downwind.

Table 2. Aerocet-531S Mass Particle Counters main characteristics.

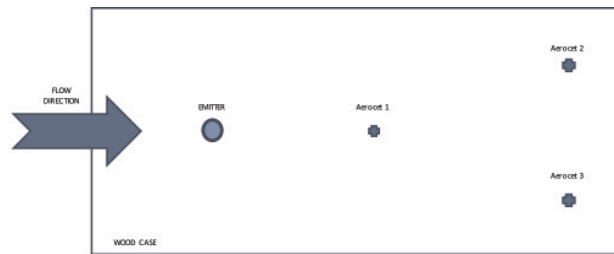| Specifications	Value
Particle counter sizes	0.3 μm, 0.5 μm, 1 μm, 5 μm, 10 μm
Mass ranges	PM_1, $PM_{2.5}$, PM_4, PM_7, PM_{10}, TSP
Concentration range	0 – 100,000,000 particle/m^3
Accuracy	± 10% to calibration aerosol
Sensitivity	High 0.3 μm, Low = 0.5 μm
Flow rate	2.83 10^{-3} m^3/min
Sample time	60 s
Light source	Laser Diode, 90 mW, 780 nm

Fig. 1. Experimental set-up

3. CFD 3D modeling strategy

The CFD model was implemented in ANSYS Fluent. A 3D CAD of the experimental set up was generated placing the emitter, the Aerocet sensors and the obstacle, when present, as reported in Fig. 2. The computational domain had the dimensions of the wind tunnel where the experiments were carried out. The test section of the wind tunnel is a box of 1.2 m x 0.5 m x 0.5 m.
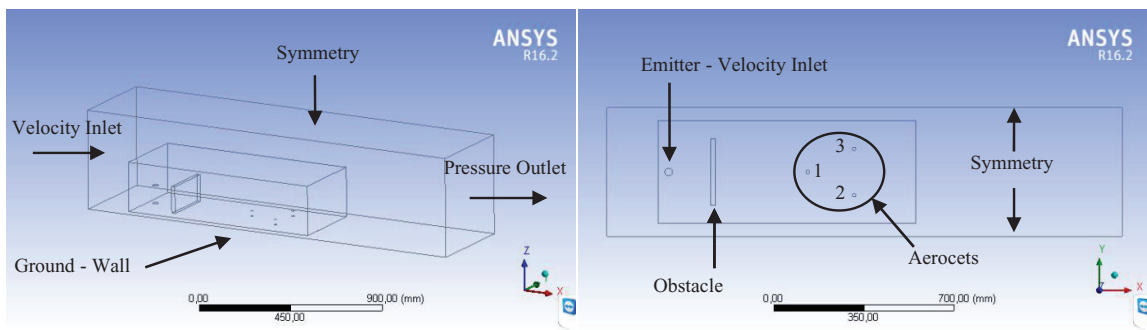

Fig. 2. Computational domain and boundary conditions with box for meshing refinement. 3D view (left), upper view (right)

The grid was constructed using ANSYS Meshing. As the particulate transport and diffusion took place near the emitter in the flow direction. The domain was splitted adding a box in order to locally refine the mesh. Three levels of refinement were tested in order to obtain a grid independent solution. A local volume sizing control was thus used with three different level of the element sizes: 0.005 (grid 1), 0.0025 (grid 2) and 0.001 m (grid 3). The grids were subsequently converted in ANSYS Fluent from a tetrahedral to a polyhedral geometry in order to reduce the interpolation errors and the number of cells, speeding up the calculation as well. The optimal compromise for a grid independent solution was found with a volume element dimension inside the box of 0.0025 m thus resulting in a tetrahedral grid with near 34 million cells, subsequently converted into 6 million polyhedral cells. A detail of the polyhedral mesh is presented in Fig. 3. Specifically, the grid independence study was done carrying out simulations with all the three refinement levels, evaluating the concentration on the aerocet 1. As the difference in calculated PM_{10} concentration on erocet 1, between grid 2 and 3, was negligible, the grid 2 (0.0025m) was chosen for all the calculations.
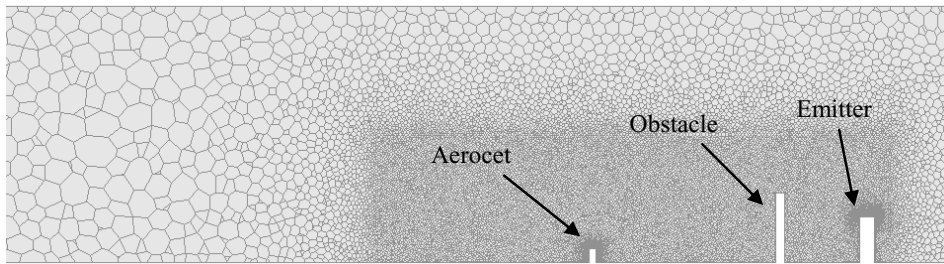
Fig. 3. Detail of the polyhedral mesh near the emitter

At the beginning, the Fluent solver set-up was implemented for the condition without obstacle in order to validate the model with experimental data. Specifically, a Discrete Phase Model (DPM) was used for simulating the PM_{10} injection and dispersion. The DPM is based on a Eulerian approach for the continuous phase and a Lagrangian approach for the discrete phase. The interaction between discrete and continuous phases was taken into account by the DPM along with an unsteady particle tracking with a particle time step of 10^{-3} s. A Runge-Kutta high order scheme was used for tracking particles. The injection of the carbon discrete phase was set at the upper face of the emitter with a particle diameter of 10^{-5} m (PM_{10}), a velocity magnitude of 0.6 m/s and a particulate mass flow rate of 10 µg/s, as obtained in the experiments. The turbulent dispersion was implemented by means of a stochastic tracking in a discrete random walk model with a time scale constant of 0.001 s.

Two different turbulent models were tested. A steady RANS Realizable k-ε for the simulations without obstacles and a quite accurate Unsteady Detached Eddie Simulation (DES) for a better modeling of the wake and recirculation areas around the obstacle. This is of great importance in order to obtain an accurate evaluation of the PM_{10} concentrations generated by the turbulent wake. The DES model is based on a RANS formulation for the boundary layer and a LES formulation for the outer zones, where the flow field is dominated by the large scales eddies. The DES model was implemented with a Realizable k-ε formulation for the RANS zones, using a time step of 0.005 s.

For both conditions, with and without obstacle, a coupled pressure-velocity solver was used with a second order upwind spatial discretization scheme for all equations. The simulations were performed on a Fujitsu Primergy TX200 S5 Server, with 2 Intel Quad Core Xeon X5570 processors (2.93 GHz) and 48 GB of RAM memory installed. A METIS parallel computing technique was thus implemented, partitioning the grid on the 16 available threads. Twenty seconds of flow were simulated, as it was evaluated enough, for sampling mean values of PM_{10} concentrations. Nearly 30 hours were needed for simulating 20 s in the steady RANS simulation without obstacles and at least 100 hours with the unsteady DES simulation. In the last condition, the computation time is considerably high and for this reason, at the state, only one configuration, with an obstacle 1.5L high at a distance of 2L from the emitter and at four different flow speed (2, 3, 4 and 5 m/s) was simulated.

4. Results and discussion

As far as the experimental results is concerned, different tests were carried out using the described experimental set-up. It is possible to observe in Fig. 4, that the PM concentration in Aerocet 1 (Fig. 4a), Aerocet 2 (Fig. 4b) and Aerocet 3 (Fig. 4c) grows when the emitted PM mass flow rate increases and decreases when the air velocity increases.
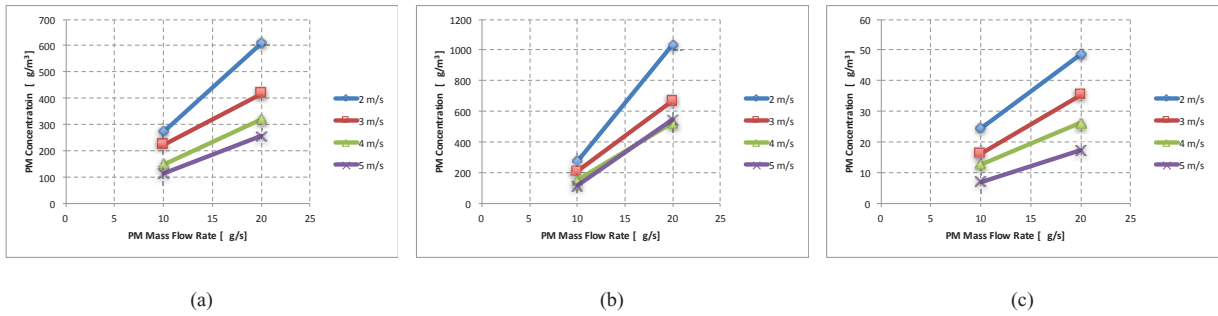
Fig. 4. (a) PM_{10} concentration of Aerocet 1 versus Emitter PM_{10} mass flow rate and wind velocity; (a) PM_{10} concentration of Aerocet 2 versus Emitter PM_{10} mass flow rate and wind velocity; (a) PM_{10} concentration of Aerocet 3 versus Emitter PM_{10} mass flow rate and wind velocity;

First, the CFD simulations were carried out for the steady state case without the obstacle in order to validate the model. As can be observed in Table 3, the prediction of the PM_{10} concentration for the Aerocet 1 and 3 (Fig. 2) shows a good correlation with the experimental data for all the flow speed thus demonstrating the high reliability of the DPM CFD 3D model.

The high predictive capabilities of the PM_{10} dispersion allowed the authors to use this CFD strategy to support the experiments and validate simplified models. In Fig. 5 contours of particulate concentration and streamlines of the flow speed from the emitter demonstrate the gravity effects on particulate dispersion and local recirculation phenomena related to the wake detached from the emitter and Aerocets.

Table 3. Numerical and Experimental PM10 concentrations.

Parameter	PM_{10} Concentration [μg/m³]											
	Aerocet 1				Aerocet 2				Aerocet 3			
Flow Velocity at inlet [m/s]	2	3	4	5	2	3	4	5	2	3	4	5
Experiments without obstacle	275	224	150	114	-	-	-	-	25	16	13	7
CFD RANS without obstacle	269	231	138	106	22	14	12	6	21	14	12	5
CFD DES with obstacle	221	108	87	62	188	122	86	65	185	124	87	63

As mentioned above, a powerful unsteady DES simulation was carried out for the test case with the obstacle. The results showed a particular trend. As the flow speed increases, the concentration on the Aerocets decreases and it also proves true for the case without the obstacle. The reason for this, is related to the increase of the momentum of the particle with speed and to the fact that the wake expands with speed.

The recirculation area around the obstacle is thus of the utmost importance for the correct evaluation of the transport and dispersion of the particulate. The use of the DES turbulence model is needed when it is necessary to accurately predict the interaction between obstacles and flow field. Furthermore, the Aerocets 2 and 3 showed a symmetrical dispersion with a great increase compared to the case without obstacles and a decrease in the concentration lower than in the Aerocet 1.

This is presented in the chart in Fig. 6 while in Fig. 7, the comparison between velocity streamlines at the different flow speed shows the increase in recirculation area behind the obstacle.
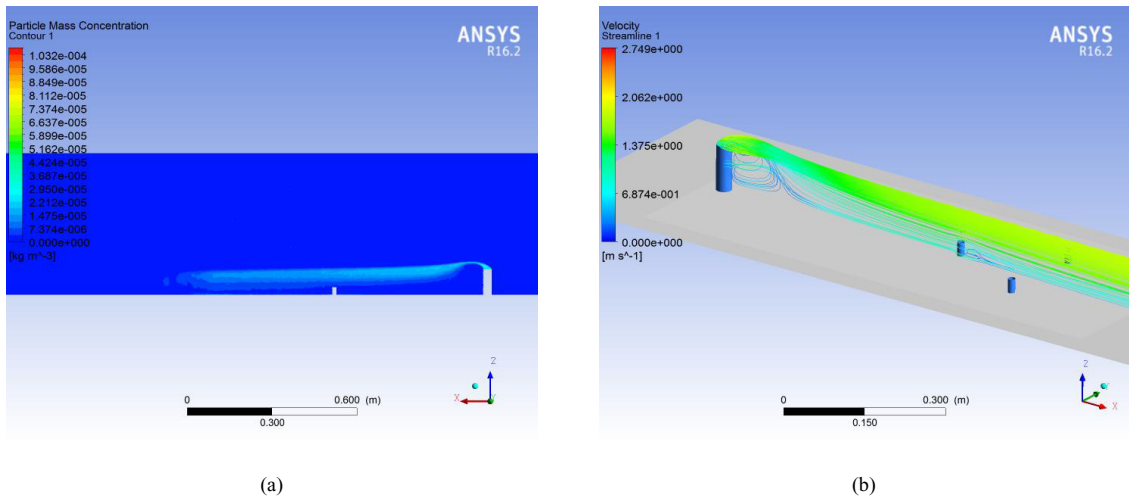
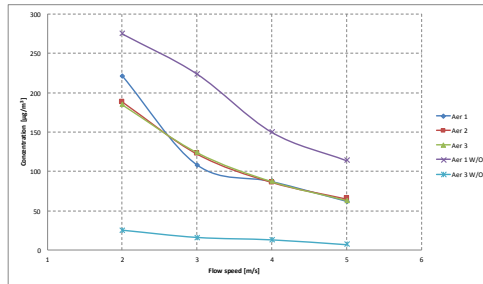Fig. 5. (a) Contours of PM$_{10}$ concentration; (b) velocity streamlines

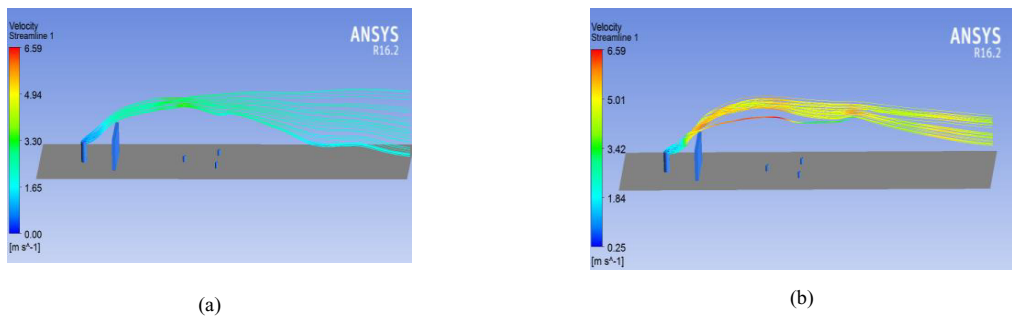Fig. 6. Trend of the particulate concentration in function of flow speed.

Fig. 7. (a) Streamlines of flow velocity from the emitter at velocity inlet of 2 m/s; (b) Streamlines of flow velocity from the emitter at velocity inlet of 4 m/s.

In conclusion, the analysis presented in this paper deals with an in scale evaluation of the phenomena related to PM$_{10}$ dispersion. It is straightforward that in real scale, with real obstacles and emitters, the effects of the little

turbulence scales become less and less important. The boundary layer behavior will be thus less significant while the larger scale eddies will become predominant. The use of the DES turbulence model, however, thanks to the LES formulation, will allow the solver to capture the main large scale effects, responsible for the particulate transport and diffusion. The aforementioned results are thus significant even for the comprehension of the real scale dispersion phenomena.

5. Conclusions

In the present paper a study of PM_{10} dispersion by means of 3D CFD models was carried out. Coupled Eulerian and Lagrangian approaches were used to simulate continuous and discrete phase, respectively. The models were calibrated using experimental results obtained by means of specific setup in wind tunnel. The comparison between experimental and numerical results highlight that the model is able to describe both flow field and particulate matter dispersion correctly. Therefore, the model could be considered calibrated. Using the implemented CFD model, a fluid-dynamic study of the flow field in the control volume around obstacles was carried out to understand how obstacles influence PM dispersion in the atmosphere. A constant PM mass flow rate was imposed at the emitter while the air velocity was varied between 2 and 5 m/s. On the basis of the results, the obstacle acts as a sort of PM concentration multiplier. In fact, analyzing the results with and without the obstacle it is possible to observe a PM concentration increment with the obstacle. This behavior is observed at all imposed air velocity. The registered PM concentration increment with the obstacle is probably a consequence of recirculation phenomena generated around the obstacles. A big eddy is observed very close to the obstacle that drops to the ground particulate matter. The presented results highlight the intimate link between geometrical parameters, pollutant amount, wind intensity and direction. Moreover, the present study represents the basis to understand the pollutant sources interaction with natural and artificial barriers to preserve urban areas from noxious substances concentration.

References

[1] Ezzati M, Kammen DM. Quantifying the effects of exposure to indoor air pollution from biomass combustion on acute respiratory infections in developing countries. Enviromental Health Perspectives 2001; 109(5): 481-488.
[2] Brusca S, Lanzafame R, Marino Cugno Garrano A, Messina M. Dynamic analysis of combustion turbine running on synthesis gas. International Journal of Applied Engineering Research 2015, 10(21): 42244-42253.
[3] Brusca S, Lanzafame R, Marino Cugno Garrano A, Messina M. Effects of pressure, temperature and dilution on fuels/air mixture laminar flame burning velocity. Energy Procedia 2015; 82: 125-132.
[4] Brusca S, Chiodo V, Galvagno A, Lanzafame R, Marino Cugno Garrano A. Analysis of reforming gas combustion in Internal Combustion Engine. Energy Procedia 2014, 45: 899-908.
[5] Famoso F, Lanzafame R, Monforte P, Oliveri C, Scandura PF. Air quality data for Catania: Analysis and investigation case study 2012-2013. Energy Procedia 2015; 81: 644-654.
[6] Lanzafame R, Scandura PF, Famoso F, Monforte P. NO2 concentration analysis in urban area of Catania. Energy Procedia 2014; 45: 671-680.
[7] Yu H, Stuart AL. Exposure and inequality for select urban air pollutants in the Tampa Bay area. Energy Procedia 2016; 551-552: 474-483.
[8] Holmes NS, Morawska L. A review of dispersion modelling and its application to the dispersion of particles: An overview of different dispersion models available. Atmospheric Environment 2006; 40: 5902-5928.
[9] Di Sabatino S, Buccoleri R, Pulvirenti B, Britter R. Simulations of pollutant dispersion within idealized urban-type geometries with CFD and integral models. Atmospheric Environment 2007; 41: 8316-8329.
[10] Mavroldls I, Andronopoulos S, Venetsanos A, Bartzls JG. Numerical investigation of concentrations and concentration fluctuations around isolated obstacles of different shapes. Comparison with wind tunnel results. Environ Fluid Mech 2015; 15: 999-1034.
[11] Brusca S, Lanzafame R, Messina M. Low-speed wind tunnel: design and build. Wind Tunnels: Aerodynamics, Models and Experiment 2001. p. 189-220.
[12] Brusca S, Famoso F, Lanzafame R, Marino Cugno Garrano A, Monforte P. Experimental analysis of a plume dispersion around obstacles. Energy Procedia 2015; 82:695-701.
[13] Elseth J. Aerocet-531S Mass Particle Counters User Manual. Met One Instruments 2013. p. 1-32.
[14] Tallini A, Vallati A, Cedola L. Mobile platform of SRF production and electricity and heat generation. Energy Procedia 2015; 82:841-847.
[15] De Lieto Vollaro R, Faga F, Vallati A, Tallini A, Cedola L. Energy and thermodynamical study of a small innovative compressed air energy storage system (micro-CAES). Energy Procedia 2015; 82:645-651.
[16] Tallini A, Vallati A, Cedola L. Applications of micro-CAES systems: energy and economic analysis. Energy Procedia 2015; 82:797-804.
[17] Vallati A, De Lieto Vollaro R, Tallini A, Cedola L. Photovoltaics noise barrier: acoustic and energetic study. Energy Procedia 2015; 82:716-723.